PCCP

ROYAL SOCIETY OF CHEMISTRY

PAPER

Cite this: *Phys. Chem. Chem. Phys.*, 2020, **22**, 14088

Theoretical characterization of the electronic properties of heterogeneous vertical stacks of 2D metal dichalcogenides containing one doped layer†

Amine Slassi, David Cornil and Jérôme Cornil *

Received 7th April 2020,
Accepted 29th May 2020

DOI: 10.1039/d0cp01878c

rsc.li/pccp

The rise of van der Waals hetero-structures based on transition metal dichalcogenides (TMDs) opens the door to a new generation of optoelectronic devices. A key factor controlling the operation and performance of such devices is the relative alignment of the band edges of the components. The electronic properties of the layers can be further modulated by chemical doping, typically leading to the introduction of gap states. However, it is not clear whether the impact of doping in a given layer is preserved when building vertical stacks incorporating it. This has motivated the present study aiming at shedding light by means of first-principles calculations on the electronic properties of heterogeneous bilayers containing one doped layer. Doping has been achieved based on the experimental literature by inserting the dopants by substitution in the 2D layer, by covalently attaching adatoms or functional groups on the surface, or by physisorbing electroactive molecules. Interestingly, very different scenarios can be encountered depending on the two materials present and the nature of doping. The impact of doping is preserved when the trap levels associated with the dopants lie in the bandgap of the bilayer. On the other hand, the pristine neutral layer can get doped to an extent depending on how its electrons can fill the trap levels associated with the other component. Altogether, the present theoretical work demonstrates that the properties of the bilayers are not simply defined by additive rules of the components.

I. Introduction

Two-dimensional materials, such as graphene, black phosphorus and transition metal dichalcogenides (TMDs), are emerging as exciting materials for new generations of atomically thin (opto)electronic devices including photodetectors,[1] ultrafast lasers,[2] field-effect transistors,[3,4] photovoltaic cells,[5,6] and optical modulators.[7,8] This interest stems from their attractive properties such as direct bandgaps exploitable in light-emission processes and strong light–matter interactions in the visible range.[5,9] Another unique feature of such structures is to allow for the fabrication of devices by creating vertically stacked hetero-structures made of individual sheets interacting by van der Waals interactions.[10] In recent years, a variety of hetero-structures such as graphene/MoS_2,[11] aluminum nitride (AlN)/MoS_2,[12,13] and TMD/TMD have been assembled for various applications.[14–16]

In all cases, the energetic alignment of the valence and conduction band edges at interfaces is a key parameter controlling the device performance, which is governed by interfacial electronic effects such as charge transfer and/or charge redistribution (polarization) effects.[17,18] For photovoltaic applications, a type-II band alignment between the two materials (with the bottom of the conduction band and the top of the valence band of the full system localized on the donor and acceptor sheets, respectively) is required to promote exciton dissociation.[19] Heterostructures in such type-II band alignment based on WS_2/MoS_2 and WSe_2/MoS_2 stacks have been used in optoelectronic applications such as direct photocatalysis,[20] photodiodes,[21,22] or transistors.[23] A key issue here is to assess whether the energy of the band edges of the individual sheets remains unaffected by the vertical stacking. In this context, our recent calculations performed on representative stacks including MoS_2 as the acceptor and $MoSe_2$, WS_2 and WSe_2 as the donor suggest that band edges can be shifted by as much as 0.3 eV by hybridization or charge-transfer effects at interfaces.[14] On the other hand, strategies involving chemical doping or tensile/compressive strain at interfaces have been exploited to modulate the properties of hetero-structures. For instance, Wang *et al.* reported a high-performance phototransistor based on a p-doped WSe_2 layer ($Nb_{0.005}W_{0.995}Se_2$) deposited on an un-doped WSe_2 layer.[24] Similarly, the introduction of C dopants (C substituting for N) in AlN interfaced with MoS_2 induces significant

Laboratory for Chemistry of Novel Materials, University of Mons, BE-7000 Mons, Belgium. E-mail: jerome.cornil@umons.ac.be

† Electronic supplementary information (ESI) available. See DOI: 10.1039/d0cp01878c

modifications in the electronic structure and changes the band alignment from type-I (with the valence and conduction band edges of the full system localized on the same layer) to a type II configuration.[12] Instead of introducing dopants directly within the 2D layer, an alternative approach to dope TMD monolayers is to have electron acceptor/donor molecules physisorbed on the surface (basal plane).[25–28] This surface doping allows preserving the pristine geometric structure of the nanostructures and may help in the exfoliation process. For instance, the functionalization of single layer TMDs with the TTF donor [TCNQ acceptor] molecule yielded n [p]-type doping by electron transfer from [toward] the adsorbed molecules.[25–27] Both experimental measurements and theoretical calculations further demonstrated that even small aromatic solvent molecules can also locally modify the electronic properties of TMD monolayers.[28] A third approach to trigger n-/p-type doping is to introduce adatoms on the surface.[29–36]

In this context, the main goal of the present study is to assess whether the changes induced in the electronic properties of a 2D TMD layer by doping are preserved when building a hetero-structure incorporating it, an issue that has received little attention so far to the best of our knowledge. We will focus on WS_2/MoS_2 and WSe_2/MoS_2 structures as representative TMD/TMD hetero-structures, in which WS_2 or WSe_2 plays the role of the donor layer while MoS_2 plays the role of the acceptor layer. The introduction of n-type or p-type characteristics has been achieved by various approaches: molecular adsorption, adatoms or substitutional doping. An n-type character is given to WS_2 or WSe_2 to add extra electrons and increase the donor character while p-type doping will be applied to MoS_2 to remove electrons and therefore make it more electron accepting.

II. Computational methods

First-principles calculations have been performed at the Density Functional Theory (DFT) level. The ion–electron interactions are treated within the projector augmented wave (PAW) scheme for a basis set,[37] as implemented in the plane-wave VASP code (Vienna *ab initio* simulation package). Since the local-density approximation (LDA)[38,39] is found to yield lattice constants and interlayer distances for TMDs in good agreement with available experimental data,[40,41] it is used here to describe the exchange–correlation contributions. We emphasize that the LDA does provide direct bandgaps much smaller by a few tenths of an eV compared to GW[42] or DFT/HSE03 calculations;[14] however, the relative band alignment of prime focus in our work is qualitatively depicted at the LDA level, thus motivating this choice to avoid extensive computational times. A kinetic energy cutoff of 530 eV was chosen for the plane-wave expansion of wave functions and a $4 \times 4 \times 1$ Monkhorst–Pack scheme of k-point sampling was adopted for the integration over the first Brillouin zone. Gaussian smearing with a width of 0.01 eV was used to determine the partial occupancies for each band (the Fermi-smearing and tetrahedron

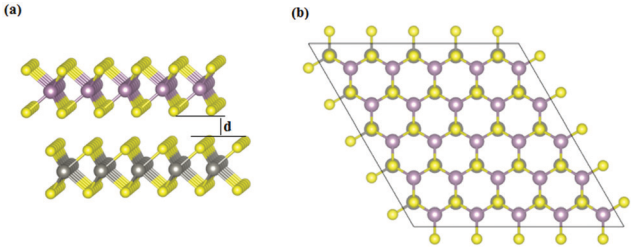

Fig. 1 (a) Side and (b) top views of the $5 \times 5 \times 1$ supercell of the WS_2/MoS_2 bilayer, respectively. d denotes the interlayer distance between the topmost atom of WS_2 and bottommost atom of MoS_2.

methods were also tested, leading to similar results). Due to the use of periodic boundary conditions, a vacuum space of 25 Å is applied along the z stacking direction (*i.e.*, normal to the interface), which is large enough to avoid interactions between adjacent layers. A supercell made of 5×5 units was employed in the basal plane. Charge transfer effects are described using Bader analysis. The spin–orbit coupling is not taken into account in these calculations. One main effect of the spin–orbit coupling is to induce a band edge splitting at some high symmetry points of the band structure.[43] This is not expected to impact our study primarily focused on the shift of electronic levels when building hetero-structures.

For TMD layers, although several polymorphs are known, we only consider the 2H form here as it is the most stable one according to previous works.[44,45] Moreover, the AB stacking, *i.e.*, with the chalcogen atoms of one layer on top of the metal atoms of the other layer (see Fig. 1), was chosen as it is more energetically stable compared to the AA stacking.[46] The electronic and maximum forces between atoms converged down to 1×10^{-4} eV and 1×10^{-3} eV Å^{-1}, respectively.

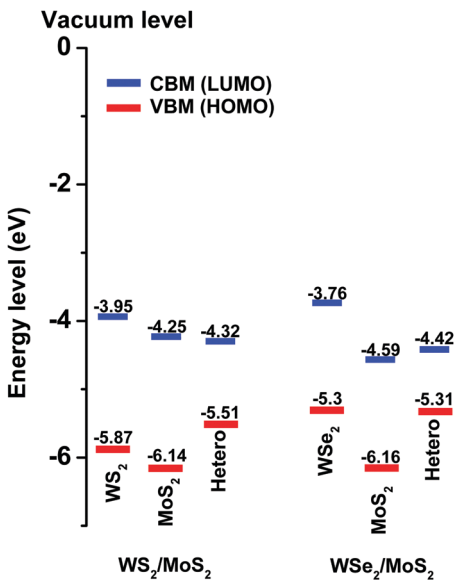

Fig. 2 Band alignment in the two bilayers, as calculated at the LDA level together with the calculated values of the VBM and CBM for the isolated sheets in the geometry of the bilayer. All energies are in eV.

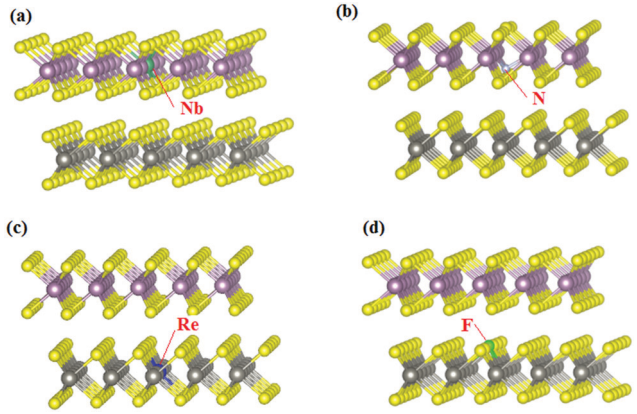

Fig. 3 Supercells of the WS_2/MoS_2 hetero-structure with (a) Nb- (b) N-, (c) Re- and (d) F-doping.

III. Results and discussions

1. Pristine systems

Before discussing specific chemical doping effects, we first briefly describe the properties of the pristine fully optimized monolayers of MoS_2, WS_2 and WSe_2 and of the MoS_2/WS_2 and MoS_2/WSe_2 bilayers. The calculated lattice constants and interlayer distances are listed in Table S1 (ESI†) and are consistent with previous calculations.[41] In the optimized bilayer geometry, the layers undergo a very small strain (0.1% and 2% for MoS_2 in WS_2/MoS_2 and WSe_2/MoS_2, respectively) due to the small lattice mismatch; strain effects are thus not expected to play a major role in the trends discussed hereafter.

We have also computed the binding energy between the two layers in WS_2/MoS_2 and WSe_2/MoS_2 hetero-structures as:

$$E_b = E_{tot} - E(WX_2) - E(MoS_2) \quad (1)$$

where E_{tot}, $E(WX_2)$ and $E(MoS_2)$ represent the total energy of the heterostructure, WX_2 monolayer (X = S or Se), and MoS_2, respectively. By definition, a negative E_b indicates that the adsorption is thermodynamically favorable. The adhesion energies per $5 \times 5 \times 1$ supercell are calculated to be -2.83 and -3.05 eV for WS_2/MoS_2 and WSe_2/MoS_2, respectively.

The band structure of the bilayer points to a type-II alignment, with the CB edge localized on MoS_2 and the VB edge on WS_2 or WSe_2; the corresponding band structures are shown in Fig. S1 (ESI†). In particular, we note that the VB edge in the WS_2/MoS_2 bilayer is shifted upward by 0.3 eV compared to the individual sheets; this originates from hybridization effects linked to the small energy separation between the VB edges

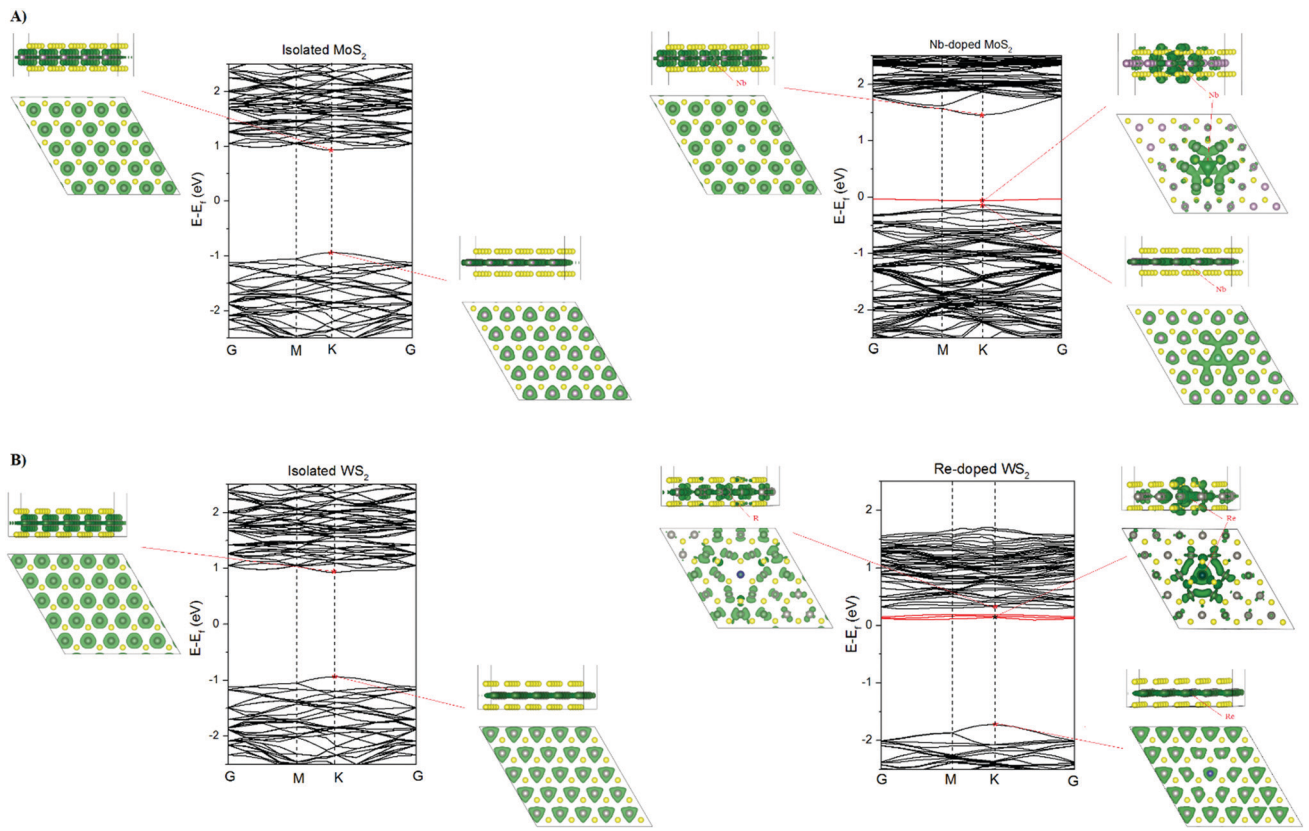

Fig. 4 (A) Band structure of a pristine MoS_2 monolayer and of the layer with a substitutional Nb dopant showing the appearance of trap states (in red) in the bandgap; (B) band structure of a pristine WS_2 monolayer and of a layer with a substitutional Re dopant showing the appearance of trap states in the bandgap. The position of the dopant is indicated by a red arrow in the orbital patterns. The trap states are mainly localized on the dopant and neighboring atoms. The orbital patterns have been generated with an isosurface value of 0.0003 e $Å^{-1}$.

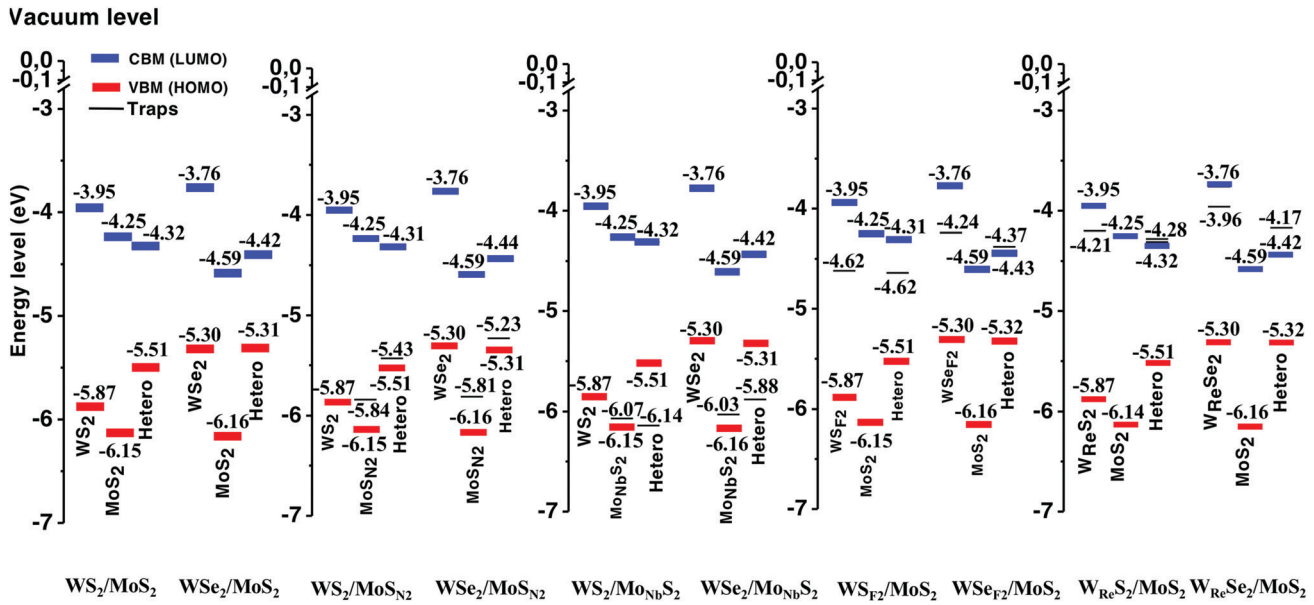

Fig. 5 Alignment of the band edges of the valence, conduction, and trap bands in the bilayers for the different doping scenarios.

of the two sheets. On the other hand, the CB edge of MoS_2 is shifted downward by about 0.2 eV in the WSe_2/MoS_2 bilayer as a result of a pronounced charge transfer of $0.37|e|$ per supercell from WSe_2 to MoS_2 (by comparison the charge transfer is $0.03|e|$ in WS_2/MoS_2). These trends perfectly match those previously obtained by DFT calculations performed with the HSE03 functional.[14]

2. Substitutional n- and p-type doping

Substitutional doping with group V elements such as Niobium (Nb) in MoS_2 has been experimentally shown to result in stable p-type doping,[47–49] whereas electron donors such as Rhenium (Re) promotes n-type doping according to DFT calculations.[48] Both theoretical calculations and high resolution scanning transmission electron microscopy (STEM) studies indicate that the Nb-atoms are substitutionally incorporated into MoS_2 by replacing the Mo-cations in the host lattice instead of dopants occupying interstitial or anti-sites.[47,48] Experimental electrical characterization shows that nitrogen atoms (N) as dopants easily substitute S-sites in the MoS_2 structure, as further confirmed by first-principles calculations, both pointing to a p-type character.[48,50,51] Accordingly, we induce here n-doping in the donor WS_2 (WSe_2) layer *via* fluorine atoms F (S_F: F substituting S and Se) and Re atoms (W_{Re} – Re has one extra valence electron compared to W) or p-type doping in the acceptor MoS_2 *via* N (S_N) and Nb (Mo_{Nb}: Nb has one less valence electron compared to Mo) dopants. The supercell models used for bilayers with substitutional doping are displayed in Fig. 2. The substitution of Mo or W results in a doping concentration of 4% in the 5×5 supercell while the exchange of S or Se by F or N is achieved with a concentration of 2%. For reference, Azcatl *et al.* synthesized a 2D N-doped MoS_2 sample with a doping concentration up to 8%, thus in line with our doping concentration (Fig. 3).[50]

Doping results in a slight decrease in the lattice constants (by 0.1–0.3%) for F, N, and Re compared to a slight increase (0.7%) upon Nb doping. All relevant structural parameters of the doped monolayers and bilayers are shown in Table S2 (ESI†). Interestingly, the interlayer distances are reduced (by 0.7–2.9%) in all doped bilayers compared to the pristine systems. This is explained by a systematic increase in the amount of interfacial charge transfer when introducing a doped layer in the bilayer (by up to a factor of 6, see Table S3, ESI†), and thus an increase in Coulomb attraction between the two sheets.

The substitutional doping brings a significant change in the electronic properties of the individual monolayers, as illustrated in Fig. 4 for MoS_2 with a Nb dopant and WS_2 with a Re dopant; the band structures associated with the other dopants show similar trends and are shown in Fig. S2 (ESI†). In all cases, trap bands are introduced in the bandgap and correspond to localized states obtained by hybridization of the orbitals of the dopant and those of the neighboring atoms (see Table S4, ESI†). In theory, the trap states should be half filled due to the odd number of electrons promoted in the unit cell upon doping. This is clearly the case for Re and F atoms leading to an n-type doping revealed by the appearance of shallow states below the conduction band edge of WS_2. F doping actually leads to the appearance of a half-filled state (occupied by 50%) localized 0.67 eV below the CBM (Conduction Band Minimum) and an empty state localized 0.16 eV below it. Re doping promotes the creation of nearly degenerate shallow states (separated in 3 states) localized 0.15 eV below the CBM. The total contribution of the Re atom in the trap states amounts to 26.3% within the three separated states while the contribution of F is 8.4% in the half-filled state and 4.3% in the empty state, thus evidencing the strong hybridization with the atoms of the 2D layer; these numbers have been obtained

by projecting the wave functions onto spherical harmonics (centered at the position of the ions) for each band. In the case of N doping, a single half-filled trap band appears 0.30 eV above the valence band edge of MoS_2, with a weight on the N atom of ~15%. A single trap band filled at 58% is obtained upon Nb doping, with a contributing weight of 12% on the dopant. The deviation from 50% implies that the orbitals of the impurity are more mixed with the orbitals of the MoS_2 sheet, in consistency with the spin-polarized LDA calculations in ref. 48, even pointing to a diamagnetic character.[48] Note that the actual emptying of the valence band upon p-doping and filling of the conduction band upon n-doping do not take place in our calculations performed at zero Kelvin. Deepak *et al.*[52] evidenced at the density-functional tight-binding (DFTB) level that Re-doped MoS_2 also leads to an n-type doping by creating shallow donor states (with a weight of 20% associated with Re), which is similar to the Re-doped WS_2 (WSe_2) picture discussed above. We stress that the same picture holds true when increasing the size of the super cell (and hence reducing the degree of doping) due to the localized character of the gap states associated with the defects, see Fig. S3 (ESI†).

The band alignment in the doped heterogeneous bilayers is shown in Fig. 5 in the presence of a p-doped acceptor; all band structures of the doped bilayers are shown in Fig. S4 (ESI†). Interestingly, the doping does not change significantly (by typically less than 0.1 eV) the positions of the VBM (Valence Band Maximum) and CBM of the layers, whereas the energy of the trap states can undergo much larger variations. In the case of Nb-doping, the trapped states are weakly shifted (by −0.07 eV) in the $WS_2/Mo_{Nb}S_2$ bilayer and by +0.15 eV in $WSe_2/Mo_{Nb}S_2$. In both cases, there is also an increase in the charge transfer from the donor to the doped acceptor (from 0.03|*e*| in WS_2/MoS_2 to 0.24|*e*| in $WS_2/Mo_{Nb}S_2$ and from 0.37|*e*| in WSe_2/MoS_2 to 0.62|*e*| in $WSe_2/Mo_{Nb}S_2$) due to the appearance of the partially occupied localized states in the bandgap of MoS_2. In this case, no trapped states are left in the bandgap of the heterojunction. The traps created by the Nb atoms are localized 0.6 eV below the VBM of the bilayer; they are fully occupied while the VB becomes partially occupied at 56% (estimated as an average for different *k*-points), thus indicating that the pristine MoS_2 layer becomes un-doped and that the doping is transferred to the donor layer in both $WS_2/Mo_{Nb}S_2$ and $WSe_2/Mo_{Nb}S_2$ hetero-bilayers. Strikingly, N-doping leads to a drastically different situation by exhibiting a huge upward shift of the trapped states (by 0.58 eV in WS_2/MoS_{N2} and in WSe_2/MoS_{N2}) which remain in the bandgap of the heterojunction. Here, since the dopant is introduced at the edge of MoS_2 in the interfacial region rather than in the middle of the MoS_2 sheet like for Nb, the trapped state gets hybridized with the valence band states of WS_2 or WSe_2, thus explaining a fundamentally different behavior; actually, ~5% of W-dz^2 and ~3% of S/Se-pz orbitals of the donor layer hybridize with the trap orbitals induced in the MoS_{N2} top layer. The occupation rate of the trap states is similar to that of the doped monolayer (50%) with almost the same weight on the N atom (16%).

In the case of the n-type doping of the donor, the electronic levels associated with the trap states induced by the Re or F dopants weakly shift in the bilayers. The electron occupation rate of the traps is hardly changed for F-doping in WS_2/MoS_2

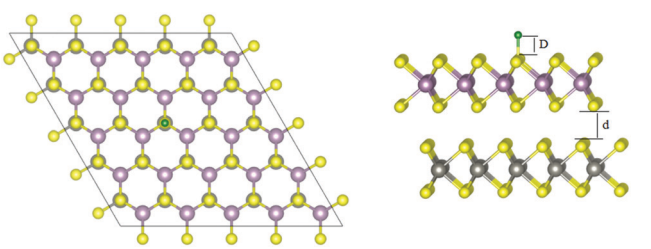

Fig. 6 Geometric structure of the WS_2/MoS_2 bilayer with R adsorbed on top of a S atom of MoS_2. *d* denotes the interlayer distance between the topmost atom of WS_2 and bottommost atom of MoS_2 while *D* denotes the bond length between the adatom and the S atom.

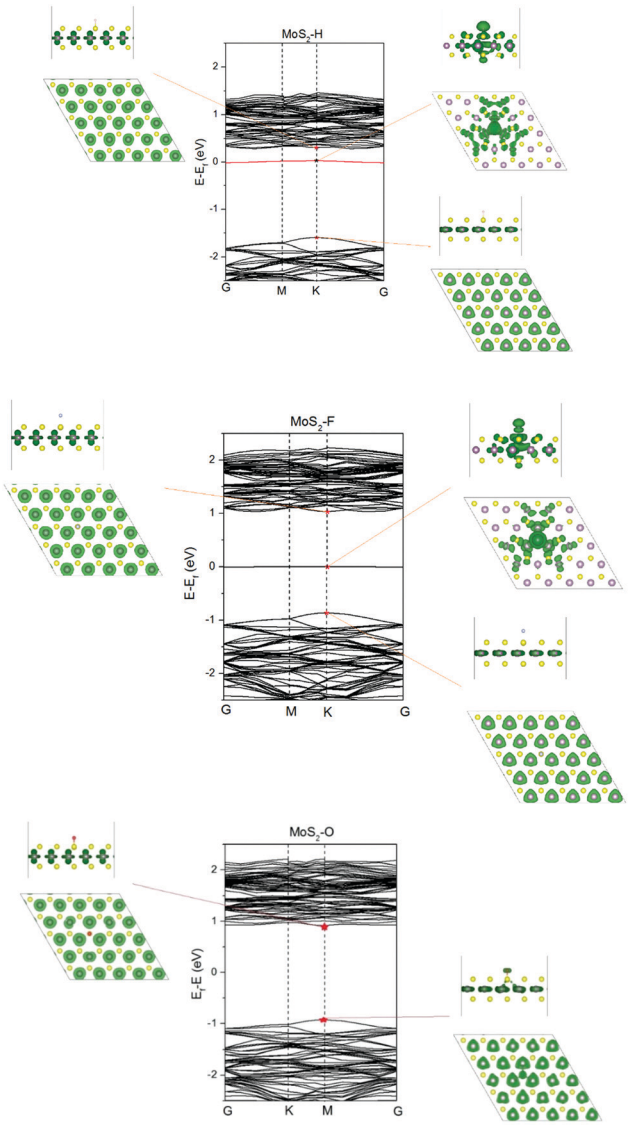

Fig. 7 Band structure of a single MoS_2 monolayer with H, F, and O adatoms. The results show the appearance of a half-filled trap band upon H and F doping. The trapped states are mainly localized on the adatom and neighboring atoms. The total contributions of the dopants in the trap levels are 5% for H, 21% for F and 6% for O adatoms.

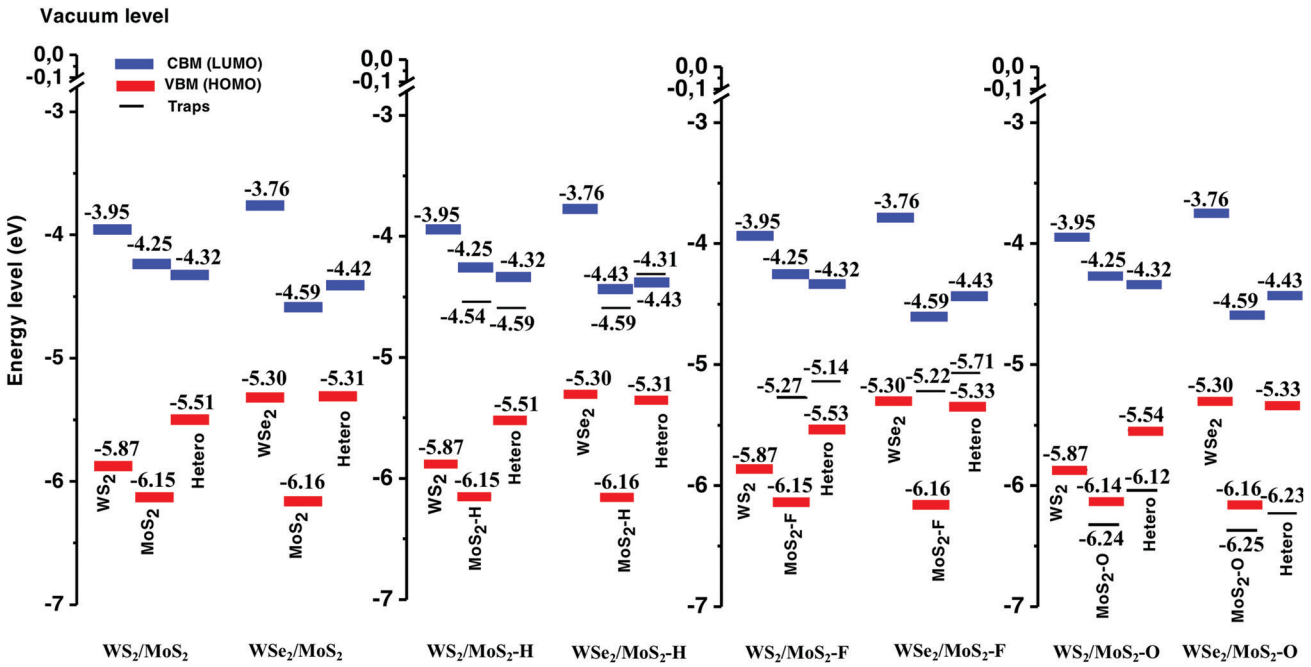

Fig. 8 Band edge alignment in the bilayers with F, O, and H doped MoS_2 compared to the pristine system. The positions of the VBM and CBM in the isolated monolayer are obtained from their actual geometry in the bilayer.

since the trapped states are not in resonance with the conduction band of MoS_2. The localization of traps above the CBM in the WSe_2/MoS_{F2} bilayer leads to a strong mixing of the levels so that the trap levels and CB become partially occupied at 25% for each, as averaged throughout the k space. The traps induced by Re-doping are localized above the CBM in both cases. The small energy separation in $W_{Re}S_2/MoS_2$ leads to a strong mixing and to trap levels partially occupied at $\sim$18% and the CBM at $\sim$32% on average. In the latter two cases, the impact of doping thus becomes distributed in the two layers. The same trend is also observed in $W_{Re}Se_2/MoS_2$ where the wider energy separation leads to the trap levels partially occupied at $\sim$8.3% and CBM at $\sim$41.4% on average. The charge transfer between the two layers is systematically increased upon introduction of trap states (see Table S3, ESI†), except for WS_{F2}/MoS_2 where the trap states in WS_2 are not in resonance with the conduction levels of MoS_2 and do not allow for downhill charge transfer processes.

3. Doping by covalent functionalization

Due to the high surface area of 2D TMD monolayers, adsorption of molecules or adatoms *via* covalent functionalization can be an effective approach for doping and band-structure engineering. The impact of chemical adsorption of different single atoms such as hydrogen (H),[30,53] oxygen (O)[31,34,35] or molecules[36] on the

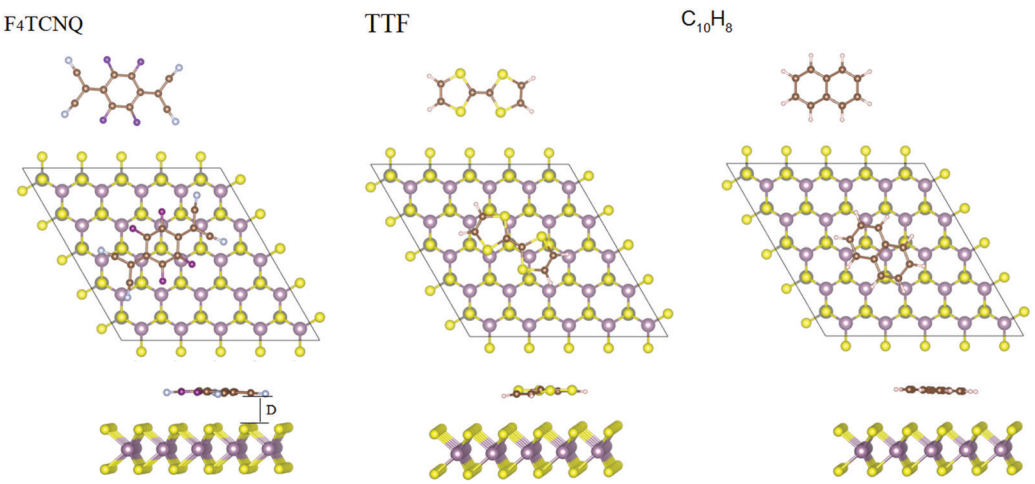

Fig. 9 Top and side views of the most favorable configuration of (a) MoS_2/TTF, (b) MoS_2/F_4TCNQ and (c) $MoS_2/C_{10}H_8$, as calculated at the LDA/DFT level. D denotes the intermolecular distance between the MoS_2 surface and the molecular plane.

electronic properties of a MoS_2 monolayer has been previously investigated. First-principles calculations lead to the conclusion that the MoS_2 monolayer should exhibit metallic, semi-metallic or semiconducting behaviors depending on the adatom types.[29] Several experimental studies have demonstrated that hydrogenation of a MoS_2 monolayer is realizable.[30] First-principles calculations have been reported on the hydrogenation of a MoS_2 monolayer with different H atom densities,[53] showing an increasing n-type doping.[35] Experimental studies also provided evidence of S–H bonds[30,54] and S–O[31] bonds formed upon O and H adsorption, respectively. Halogen adatoms (F, Cl, and Br) were found to be effective for n-type doping of MoS_2.[29] In this respect, Pan *et al.* showed by DFT calculations that the F atom is strongly adsorbed on MoS_2 with a large binding energy of about 2.0 eV and with the formation of a covalent F–S bond with a bond length of 1.74 Å.[55]

In this context, we have investigated here whether the impact of adatoms (–H, –F, –N, and –O) and covalently bonded groups ($–CH_3$ and $–CF_3$) on the electronic properties of MoS_2 is preserved when building a WS_2/MoS_2 or WSe_2/MoS_2 bilayer with the two sheets in van der Waals contact (and by introducing the adatoms away from the interface). We start here by describing the adsorption energies of the adatoms and the impact on the electronic properties of a MoS_2 monolayer. Experimental works varying the adatom densities on the MoS_2 surface have shown that a high density ($\sim$30% of the hydrogenated MoS_2 bilayer) can give rise to structural transition from the 1H-MoS_2 to 1T-MoS_2 structure.[30] Accordingly, to avoid this scenario, we adopt here a low doping density by adsorbing a single species on top of the MoS_2 5×5 supercell; this doping ratio of 4% leads to a surface doping density of 4.9×10^{-19} cm^{-2}. The optimized lattice constants of the doped layers are shown in Table S5 (ESI†); globally, the adatoms slightly distort the structural parameters, characteristic of the pristine MoS_2 monolayer. We have also computed the adsorption energy defined as the energy required to remove the adatom from the MoS_2 monolayer:

$$E_b = E_{total} - E(MoS_2) - E_{ad\text{-}atom} \quad (2)$$

where $E(MoS_2)$, $E_{ad\text{-}atom}$, and E_{total} are the total energies of the pristine MoS_2 monolayer, the adsorbed species, and the full system. It is worth stressing that various adsorption configurations are possible: T_M site (top site directly above a Mo atom), T_S site (top site directly above a S atom), and H site (hollow site above the center of hexagons). Our calculations for different surface adsorption sites indicate that all functional groups (R-) prefer to be adsorbed on top of S atoms (T_S site), as shown in Fig. 6. This is consistent with previous theoretical studies pointing to T_S as the most favorable adsorption site for O,[31,34,35] F,[32] and H.[30]

Fig. 7 displays the band-structure of MoS_2 with H, F, or O adatoms; the corresponding results for the other dopants are shown in Fig. S5 (ESI†). According to the electronic band-structure calculations, H, CH_3, and CF_3 yield n-type doping by creating shallow partially occupied (50% in all cases) trap states below the CBM, without any significant modulation in CBM and VBM energies and characters compared to the pristine

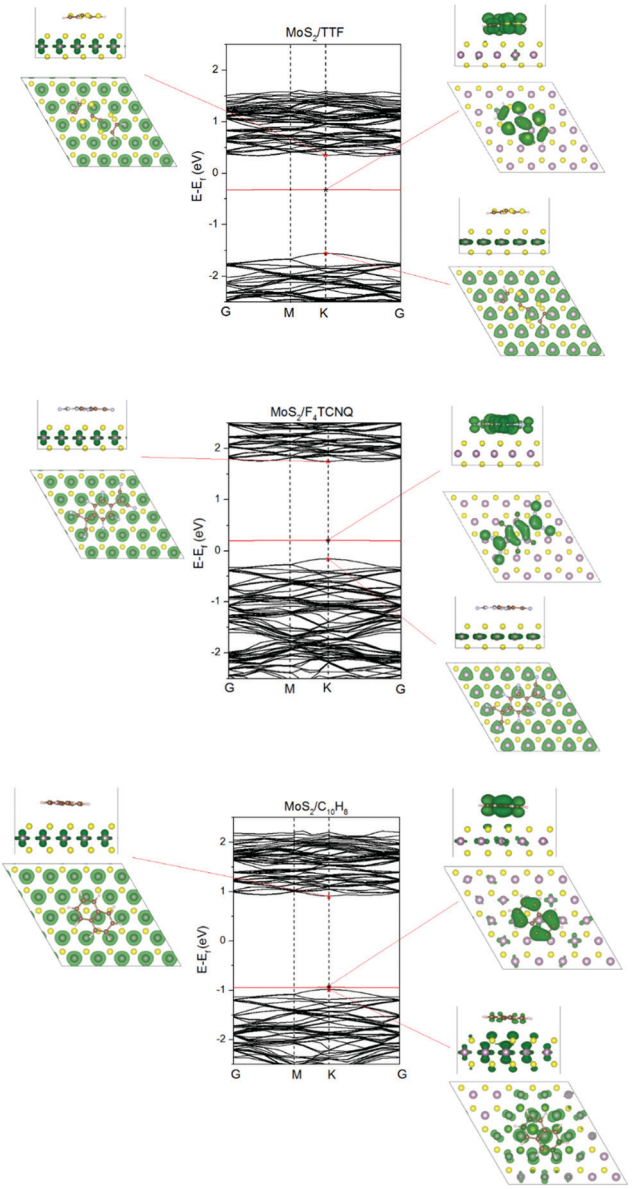

Fig. 10 Band structure of a MoS_2 monolayer showing the appearance of trap states 1.23 eV below the CBM in the presence of TTF (electron occupancy rate of $\sim$98.75%) and trap states 0.35 eV above the VBM with physisorbed F_4-TCNQ (electron occupancy rate of $\sim$7.0%) molecules. Naphthalene leads to the appearance of a fully occupied trap state close to the edge of the VBM. The total contributions of the dopants in the trap levels are 100% for TTF and F_4-TCNQ while it is only 51% for $C_{10}H_8$ due to the strong mixing with the VB.

MoS_2 monolayer (see Table S6, ESI†). In contrast, F generates partially occupied (50%) deep states 1.02 eV below the CBM while O adsorption does not induce any new state within the band gap; in the latter case, the orbital character of the VBM is slightly changed due to hybridization between the orbitals of the adatom and of the MoS_2 layer, see Fig. 7 and Table S5 (ESI†); note that a trapped state localized around the O atoms is found below the VBM in the latter case. Interestingly, the location of the trapped states does not necessarily reflect the charge transfer occurring from the dopant to the MoS_2 layer;

indeed, the states lie below the CBM for both the donor CH_3 and acceptor CF_3, whereas the charge transfer (toward MoS_2) is estimated to be $-0.11|e|$ and $+0.08|e|$, respectively (see Table S7, ESI†).

In the bilayer, the introduction of the doped monolayer does not modify significantly the interlayer distances and binding energies. Moreover, the trapped states are only weakly shifted when going to the heterogeneous structure, see the alignments of the band edges in Fig. 8 for H, F, and O doping (the other cases are depicted in Fig. S6 (ESI†) and all corresponding band-structures are provided in Fig. S7, ESI†). This is fully expected for F doping since the trapped states lie deep in the bandgap and cannot efficiently hybridize with the VBM and CBM of WS_2 and WSe_2. In the cases of H, CH_3, and CF_3 doping, shallow trap states remain in the bandgap, mostly due to the fact that (i) the defect is located away from the interface and (ii) the CBM of the two layers weakly hybridize. As a result, the amount of charge transfer between the two layers is weakly modulated by the introduction of the adatoms. Similarly, the trapped states induced by oxygen atoms remain buried in the valence band of MoS_2 in the bilayer. In these situations, the impact of doping the MoS_2 layer is thus preserved when building the vertical heterogeneous stacks.

4. Non-covalent functionalization of bilayers

A lot of theoretical and experimental efforts have been devoted to studying the interaction of TMD monolayers with different organic electroactive molecules physisorbed on their surface.[25–27] In this case, the doping can be achieved by charge transfer between the two components. In order to encompass this strategy in our study, we focus on two extreme cases by involving a very strong electron-donating molecule (tetrathiafulvalene–TTF) and a very strong electron-accepting molecule (tetrafluoro-tetracyanoquinodimethane (F_4-TCNQ)); for the sake of reference, we also consider a neutral naphthalene molecule ($C_{10}H_8$), which is neither strongly donating nor accepting electrons. The most stable contact geometries optimized at the DFT/LDA level are displayed in Fig. 9 and are consistent with previous theoretical studies using the PBE+D2 functional.[25] The key structural parameters are shown in Table S8 (ESI†). The TTF molecule is stabilized on the basal plane of MoS_2 with the two rings of TTF eclipsing two hollow rings of MoS_2. The equilibrium distance between TTF and MoS_2 is 2.71 Å and the calculated energy of adhesion defined similarly to the previous sections is -0.66 eV, close to the value of -0.67 eV obtained at the DFT/PBE+D2 level.[25] The most stable configuration for the adsorption of F_4TCNQ on MoS_2 is found when the center of the benzene ring is on top of a S atom of MoS_2. The intermolecular separation is 2.72 Å and the adhesion energy is estimated to be -0.78 eV. $C_{10}H_8$ lies flat on the surface with the center of one benzene ring on top of a S atom of the MoS_2 layer. The optimized vertical separation between the two components is 2.87 Å and the adhesion energy of -0.44 eV is lower than with TTF or TCNQ. As expected, the adhesion is stronger in the presence of a significant charge transfer ($0.22|e|$ and $0.24|e|$ for TTF and TNCQ *versus* $0.07|e|$ for naphthalene). This packing geometry is hardly modified in the bilayer whose structural characteristics are also found to be comparable to those of the pristine bi-layered systems.

Regarding the electronic structure (Fig. 10), F_4TCNQ leads to the appearance of an unoccupied band exclusively localized on the molecule (see Table S9, ESI†) and lying 0.35 eV above the

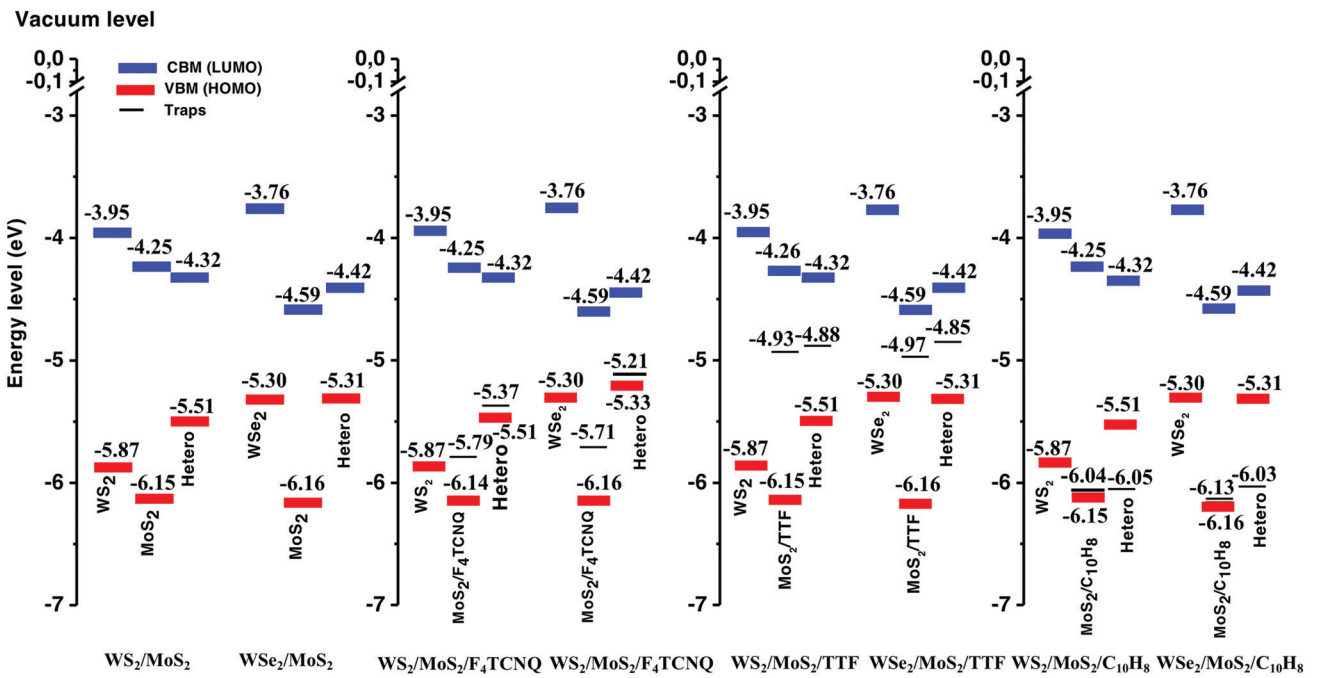

Fig. 11 Band alignment in the bilayers with MoS_2 covered by electroactive molecules. The positions of the VBM and CBM of the individual monolayers are those associated with the geometry of the full system.

VBM of MoS_2, thus rationalizing the pronounced p-type doping. For TTF, a new trap state exclusively localized on the molecule appears 1.23 eV below the CBM of MoS_2 and initiates the pronounced n-type doping. Due to the higher ionization potential of naphthalene (*i.e.*, deeper HOMO energy), the occupied trap state appearing just above the VBM originates from a mixing of the orbitals of naphthalene and MoS_2; naphthalene has thus no potential for chemical doping, as fully expected. Note that the HOMO of TTF and naphthalene [LUMO of F_4-TCNQ] is stabilized [destabilized] going from the single molecule to the physisorbed state due the loss [gain] of electrons resulting from the interfacial charge transfer (see Table S10, ESI†). The direction and amplitude of charge transfer flow is also in good correlation with the difference in chemical potential between the MoS_2 layer (−5.2 eV) and the adsorbed molecules TTF (−3.28 eV), $C_{10}H_8$ (−4.09 eV), and F_4-TCNQ (−6.72 eV), with the charges flowing from the material with the higher chemical potential to that with the lower one, with an amplitude governed by the energy difference.

Fig. 11 displays the energy level alignment in the bilayers with MoS_2 covered by the electroactive molecules; the corresponding band structures are available in Fig. S8 (ESI†). In all cases, the VBM and CBM of the bilayer are weakly affected by the molecules. For TTF, the occupied molecular levels are not shifted when building the bilayer since they lie deep into the bandgap of the full system. Similarly, the highest occupied levels of naphthalene remain at a very similar energy going from the doped monolayer to the bilayer and end up deep into the valence band of the full system. In contrast, the molecular levels of F_4-TCNQ are significantly shifted upward by as much as 0.5 eV in the bilayer. The shift of the trap state created by F_4-TCNQ is mainly due to the enhancement of charge transfer between F_4-TCNQ and the MoS_2 sheet. In the bilayer geometry, there is indeed an electron accumulation in the F_4-TCNQ molecule (with the electron occupancy of the trap evolving from 7.4% in the isolated monolayer to 19.1% in the bilayer) withdrawn from MoS_2 and WS_2 (WSe_2) layers (see in Table S10, ESI†, the amplitude of the charge for each component). In contrast, in the bilayers with TTF or C_8H_{10} adsorbed, an electron accumulation is established within the MoS_2 layer with electrons withdrawn from the molecule (TTF or C_8H_{10}) and WS_2 (WSe_2) layers.

VI. Conclusions

In summary, we have evaluated by means of DFT calculations the impact of chemical doping on the structural and electronic properties of transition metal dichalcogenide monolayers, and how the induced changes are retained when building a heterogeneous stack containing such a doped layer. We focused on prototypical TMD/TMD hetero-structures based on WS_2/MoS_2 and WSe_2/MoS_2 and promoted chemical doping by introducing substitutional dopants, grafting adatoms or functional groups, and by depositing physisorbed electroactive molecules. In all cases, the low doping ratios considered to hardly modify the geometric structure of TMDs. However, doping systematically tends to lower the interlayer distance by promoting an additional charge transfer between the two components, and hence an increased Coulomb attraction between the two sheets.

Different scenarios have been encountered as a function of materials and dopants present: (i) the electronic structure of the doped layer can remain unaltered in the bilayer; this is the case when the trap levels lie inside the gap of the bilayer; (ii) the electronic structure of the doped layer is modified when the occupation of the trap levels is modified in the bilayer due to interlayer charge-transfer processes. If the trap states get completely filled, the doping character is actually transferred to the pristine neutral layer; in intermediate cases, the two layers can become chemically doped. This work demonstrates that preserving the integrity of chemically doped 2D layers is far from being guaranteed when building vertical stacks. This does not imply, however, that the reorganization of the electronic distribution will prove always detrimental for a given application. Experimental measurements are now highly desirable to validate such predictions and help defining strategies to carefully tailor the electronic properties of vertical 2D stacks.

Conflicts of interest

There are no conflicts to declare.

Acknowledgements

This work was supported by Région Wallonie (RW), the Belgian National Fund for Scientific Research (FRS-FNRS) and Wallonie-Bruxelles International (WBI). Computational resources were provided by the Consortium des Équipements de Calcul Intensif (CÉCI) funded by F.R.S.-FNRS under Grant 2.5020.11. J. C. is an FNRS research director.

References

1 O. Lopez-Sanchez, D. Lembke, M. Kayci, A. Radenovic and A. Kis, Ultrasensitive photodetectors based on monolayer MoS_2, *Nat. Nanotechnol.*, 2013, **8**, 497.
2 F. Ceballos and H. Zhao, Ultrafast Laser Spectroscopy of Two-Dimensional Materials Beyond Graphene, *Adv. Funct. Mater.*, 2017, **27**, 1604509.
3 V. Podzorov, M. E. Gershenson, C. Kloc, R. Zeis and E. Bucher, High-mobility field-effect transistors based on transition metal dichalcogenides, *Appl. Phys. Lett.*, 2004, **84**, 3301–3303.
4 A. Slassi, P. B. Sorokin and A. Pershin, Ohmic/Schottky barrier engineering in metal/SnP_3 heterostructures, *J. Alloys Compd.*, 2020, **831**, 154800.
5 M. Bernardi, M. Palummo and J. C. Grossman, Extraordinary Sunlight Absorption and One Nanometer Thick Photovoltaics Using Two-Dimensional Monolayer Materials, *Nano Lett.*, 2013, **13**, 3664–3670.

6 M.-L. Tsai, S.-H. Su, J.-K. Chang, D.-S. Tsai, C.-H. Chen and C.-I. Wu, *et al.*, Monolayer MoS_2 Heterojunction Solar Cells, *ACS Nano*, 2014, **8**, 8317–8322.

7 B. Li, S. Zu, J. Zhou, Q. Jiang, B. Du and H. Shan, *et al.*, Single-Nanoparticle Plasmonic Electro-optic Modulator Based on MoS_2 Monolayers, *ACS Nano*, 2017, **11**, 9720–9727.

8 G. Zhao, J. Hou, Y. Wu, J. He and X. Hao, Preparation of 2D MoS_2/Graphene Heterostructure through a Monolayer Intercalation Method and its Application as an Optical Modulator in Pulsed Laser Generation, *Adv. Opt. Mater.*, 2015, **3**, 937–942.

9 L. Britnell, R. M. Ribeiro, A. Eckmann, R. Jalil, B. D. Belle and A. Mishchenko, *et al.*, Strong Light-Matter Interactions in Heterostructures of Atomically Thin Films, *Science*, 2013, **340**, 1311–1314.

10 A. K. Geim and I. V. Grigorieva, van der Waals heterostructures, *Nature*, 2013, **499**, 419–425.

11 Y. Ma, Y. Dai, M. Guo, C. Niu and B. Huang, Graphene adhesion on MoS_2 monolayer: An *ab initio* study, *Nanoscale*, 2011, **3**, 3883.

12 Q. Fang, Y. Huang, Y. Miao, K. Xu, Y. Li and F. Ma, Interfacial Defect Engineering on Electronic States of Two-Dimensional AlN/MoS_2 Heterostructure, *J. Phys. Chem. C*, 2017, **121**, 6605–6613.

13 F. Li, C. Shi, D. Wang, G. Cui, P. Zhang and L. Lv, *et al.*, Improved visible-light absorbance of monolayer MoS_2 on AlN substrate and its angle-dependent electronic structures, *Phys. Chem. Chem. Phys.*, 2018, **20**, 29131–29141.

14 A. Slassi and J. Cornil, Theoretical characterization of strain and interfacial electronic effects in donor–acceptor bilayers of 2D transition metal dichalcogenides, *2D Mater.*, 2018, **6**, 015025.

15 X. Hong, J. Kim, S.-F. Shi, Y. Zhang, C. Jin and Y. Sun, *et al.*, Ultrafast charge transfer in atomically thin MoS_2/WS_2 heterostructures, *Nat. Nanotechnol.*, 2014, **9**, 682–686.

16 A. Nourbakhsh, A. Zubair, M. S. Dresselhaus and T. Palacios, Transport Properties of a MoS_2/WSe_2 Heterojunction Transistor and Its Potential for Application, *Nano Lett.*, 2016, **16**, 1359–1366.

17 M. Linares, D. Beljonne, J. Cornil, K. Lancaster, J.-L. Brédas and S. Verlaak, *et al.*, On the Interface Dipole at the Pentacene−Fullerene Heterojunction: A Theoretical Study, *J. Phys. Chem. C*, 2010, **114**, 3215–3224.

18 I. Avilov, V. Geskin and J. Cornil, Quantum-Chemical Characterization of the Origin of Dipole Formation at Molecular Organic/Organic Interfaces, *Adv. Funct. Mater.*, 2009, **19**, 624–633.

19 M. M. Furchi, A. Pospischil, F. Libisch, J. Burgdörfer and T. Mueller, Photovoltaic Effect in an Electrically Tunable van der Waals Heterojunction, *Nano Lett.*, 2014, **14**, 4785–4791.

20 J. Shi, R. Tong, X. Zhou, Y. Gong, Z. Zhang and Q. Ji, *et al.*, Temperature-Mediated Selective Growth of MoS_2/WS_2 and WS_2/MoS_2 Vertical Stacks on Au Foils for Direct Photocatalytic Applications, *Adv. Mater.*, 2016, **28**, 10664–10672.

21 J. Lee, Y. R. Lim, A. K. Katiyar, W. Song, J. Lim and S. Bae, *et al.*, Direct Synthesis of a Self-Assembled WSe_2/MoS_2 Heterostructure Array and its Optoelectrical Properties, *Adv. Mater.*, 2019, **31**, 1904194.

22 Y. Xue, Y. Zhang, Y. Liu, H. Liu, J. Song and J. Sophia, *et al.*, Scalable Production of a Few-Layer MoS_2/WS_2 Vertical Heterojunction Array and Its Application for Photodetectors, *ACS Nano*, 2016, **10**, 573–580.

23 N. Huo, J. Kang, Z. Wei, S.-S. Li, J. Li and S.-H. Wei, Novel and Enhanced Optoelectronic Performances of Multilayer MoS_2–WS_2 Heterostructure Transistors, *Adv. Funct. Mater.*, 2014, **24**, 7025–7031.

24 T. Wang, K. Andrews, A. Bowman, T. Hong, M. Koehler and J. Yan, *et al.*, High-Performance WSe_2 Phototransistors with 2D/2D Ohmic Contacts, *Nano Lett.*, 2018, **18**, 2766–2771.

25 Y. Jing, X. Tan, Z. Zhou and P. Shen, Tuning electronic and optical properties of MoS_2 monolayer via molecular charge transfer, *J. Mater. Chem. A*, 2014, **2**, 16892–16897.

26 R. C. Selhorst, E. Puodziukynaite, J. A. Dewey, P. Wang, M. D. Barnes and A. Ramasubramaniam, *et al.*, Tetrathiafulvalene-containing polymers for simultaneous non-covalent modification and electronic modulation of MoS_2 nanomaterials, *Chem. Sci.*, 2016, **7**, 4698–4705.

27 J. Wang, Z. Ji, G. Yang, X. Chuai, F. Liu and Z. Zhou, *et al.*, Charge Transfer within the F_4 TCNQ-MoS_2 van der Waals Interface: Toward Electrical Properties Tuning and Gas Sensing Application, *Adv. Funct. Mater.*, 2018, **28**, 1806244.

28 Y. Wang, A. Slassi, M.-A. Stoeckel, S. Bertolazzi, J. Cornil and D. Beljonne, *et al.*, Doping of Monolayer Transition-Metal Dichalcogenides *via* Physisorption of Aromatic Solvent Molecules, *J. Phys. Chem. Lett.*, 2019, **10**, 540–547.

29 J. Chang, S. Larentis, E. Tutuc, L. F. Register and S. K. Banerjee, Atomistic simulation of the electronic states of adatoms in monolayer MoS_2, *Appl. Phys. Lett.*, 2014, **104**, 141603.

30 S. W. Han, W. S. Yun, J. D. Lee, Y. H. Hwang, J. Baik and H. J. Shin, *et al.*, Hydrogenation-induced atomic stripes on the MoS_2 surface, *Phys. Rev. B: Condens. Matter Mater. Phys.*, 2015, **92**, 241303.

31 A. Azcatl, S. McDonnell, K. C. Santosh, X. Peng, H. Dong and X. Qin, *et al.*, MoS_2 functionalization for ultra-thin atomic layer deposited dielectrics, *Appl. Phys. Lett.*, 2014, **104**, 111601.

32 D. Gao, S. Shi, K. Tao, B. Xia and D. Xue, Tunable ferromagnetic ordering in MoS_2 nanosheets with fluorine adsorption, *Nanoscale*, 2015, **7**, 4211–4216.

33 J. He, K. Wu, R. Sa, Q. Li and Y. Wei, Magnetic properties of nonmetal atoms absorbed MoS_2 monolayers, *Appl. Phys. Lett.*, 2010, **96**, 082504.

34 K. C. Santosh, R. C. Longo, R. M. Wallace and K. Cho, Surface oxidation energetics and kinetics on MoS_2 monolayer, *J. Appl. Phys.*, 2015, **117**, 135301.

35 L. Qi, Y. Wang, L. Shen and Y. Wu, Chemisorption-induced n-doping of MoS_2 by oxygen, *Appl. Phys. Lett.*, 2016, **108**, 063103.

36 Q. Tang and D. Jiang, Stabilization and Band-Gap Tuning of the 1T-MoS_2 Monolayer by Covalent Functionalization, *Chem. Mater.*, 2015, **27**, 3743–3748.

37 G. Kresse and D. Joubert, From ultrasoft pseudopotentials to the projector augmented-wave method, *Phys. Rev. B: Condens. Matter Mater. Phys.*, 1999, **59**, 1758–1775.

38 D. M. Ceperley and B. J. Alder, Ground State of the Electron Gas by a Stochastic Method, *Phys. Rev. Lett.*, 1980, **45**, 566–569.

39 J. P. Perdew and A. Zunger, Self-interaction correction to density-functional approximations for many-electron systems, *Phys. Rev. B: Condens. Matter Mater. Phys.*, 1981, **23**, 5048–5079.

40 T. Björkman, A. Gulans, A. V. Krasheninnikov and R. M. Nieminen, van der Waals Bonding in Layered Compounds from Advanced Density-Functional First-Principles Calculations, *Phys. Rev. Lett.*, 2012, **108**, 235502.

41 H. Terrones, F. López-Urías and M. Terrones, Novel heterolayered materials with tunable direct band gaps by sandwiching different metal disulfides and diselenides, *Sci. Rep.*, 2013, **3**, 1549.

42 A. Ramasubramaniam, Large excitonic effects in monolayers of molybdenum and tungsten dichalcogenides, *Phys. Rev. B: Condens. Matter Mater. Phys.*, 2012, **86**, 115409.

43 Z. Y. Zhu, Y. C. Cheng and U. Schwingenschlögl, Giant spin-orbit-induced spin splitting in two-dimensional transition-metal dichalcogenide semiconductors, *Phys. Rev. B: Condens. Matter Mater. Phys.*, 2011, **84**, 153402.

44 Y.-C. Lin, D. O. Dumcenco, Y.-S. Huang and K. Suenaga, Atomic mechanism of the semiconducting-to-metallic phase transition in single-layered MoS_2, *Nat. Nanotechnol.*, 2014, **9**, 391–396.

45 M. A. Py and R. R. Haering, Structural destabilization induced by lithium intercalation in MoS_2 and related compounds, *Can. J. Phys.*, 1983, **61**, 76–84.

46 J. He, K. Hummer and C. Franchini, Stacking effects on the electronic and optical properties of bilayer transition metal dichalcogenides MoS_2, $MoSe_2$, WS_2, *Phys. Rev. B: Condens. Matter Mater. Phys.*, 2014, **89**, 075409.

47 M. R. Laskar, D. N. Nath, L. Ma, E. W. Lee, C. H. Lee and T. Kent, *et al.*, p-Type doping of MoS_2 thin films using Nb, *Appl. Phys. Lett.*, 2014, **104**, 092104.

48 K. Dolui, I. Rungger, C. Das Pemmaraju and S. Sanvito, Possible doping strategies for MoS_2 monolayers: an *ab initio* study, *Phys. Rev. B: Condens. Matter Mater. Phys.*, 2013, **88**, 075420.

49 J. Suh, T.-E. Park, D.-Y. Lin, D. Fu, J. Park and H. J. Jung, *et al.*, Doping against the Native Propensity of MoS_2: Degenerate Hole Doping by Cation Substitution, *Nano Lett.*, 2014, **14**, 6976–6982.

50 A. Azcatl, X. Qin, A. Prakash, C. Zhang, L. Cheng and Q. Wang, *et al.*, Covalent Nitrogen Doping and Compressive Strain in MoS_2 by Remote N2 Plasma Exposure, *Nano Lett.*, 2016, **16**, 5437–5443.

51 X. Zhao, P. Chen, C. Xia, T. Wang and X. Dai, Electronic and magnetic properties of n-type and p-doped MoS_2 monolayers, *RSC Adv.*, 2016, **6**, 16772–16778.

52 F. L. Deepak, R. Popovitz-Biro, Y. Feldman, H. Cohen, A. Enyashin and G. Seifert, *et al.*, Fullerene-like $Mo(W)_{1-x}Re_xS_2$ Nanoparticles, *Chem. – Asian J.*, 2008, **3**, 1568–1574.

53 Y. Cai, Z. Bai, H. Pan, Y. P. Feng, B. I. Yakobson and Y.-W. Zhang, Constructing metallic nanoroads on a MoS_2 monolayer *via* hydrogenation, *Nanoscale*, 2014, **6**, 1691–1697.

54 S. Das, M. Demarteau and A. Roelofs, Nb-doped single crystalline MoS_2 field effect transistor, *Appl. Phys. Lett.*, 2015, **106**, 173506.

55 J. Pan, Z. Wang, Q. Chen, J. Hu and J. Wang, Band structure engineering of monolayer MoS_2 by surface ligand functionalization for enhanced photoelectrochemical hydrogen production activity, *Nanoscale*, 2014, **6**, 13565–13571.